Manipulation of Collective Optical Activity in One-Dimensional Plasmonic Assembly

Zhening Zhu, Wenjing Liu, Zhengtao Li, Bing Han, Yunlong Zhou, Yan Gao, and Zhiyong Tang*

Laboratory of Nanomaterials, National Center for Nanoscience and Technology, Beijing, People's Republic of China

ABSTRACT

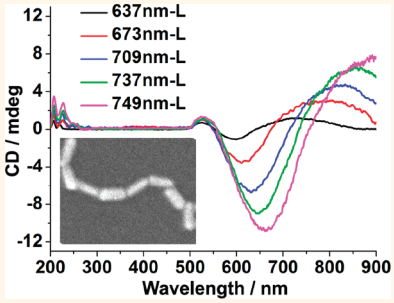

The manipulation of the chirality and corresponding optical activity in the visible—near-infrared (NIR) light region is significant to realize applications in the fields of chemical sensing, enantioselective separation, chiral nanocatalysis, and optical devices. We studied the plasmon-induced circular dichroism (CD) response by one-dimensional (1D) assembly of cysteine (CYS) and gold nanorods (GNRs). Typically, GNRs can form end-to-end assembly through the electrostatic attraction of CYS molecules preferentially attached on the ends of different GNRs. CD responses are observed at both the UV and visible—NIR light region in the 1D assembly, which are assigned to the CYS molecules and the GNRs, respectively. In addition, the wavelength of the CD responses can be manipulated from 550 nm to more than 900 nm through altering the aspect ratios of GNRs in 1D assembly. Anisotropic enhancement of optical activity is discovered, suggesting that the enhancement of the longitudinal localized surface plasmon resonance (LSPR) peak of GNRs in the CD response is much more apparent than that of the transverse LSPR. The CD responses of individual CYS-attached GNRs and CYS-assembled gold nanoparticles (GNPs) substantiate that the form of assembly and the shape of building blocks are significant not only for the intensity but for the line shape of the CD signals.

KEYWORDS: circular dichroism · gold nanorod · optical activity · self-assembly · surface plasmon coupling

Optical activity and chirality from molecules to nanoscale objects are extremely important because of their potential applications in chemical sensing,[1] enantioselective separation,[2] chiral catalysis,[3] optical materials,[4] and other nanotechnology.[5−7] Thanks to recent advances in both theoretical modeling and synthesis strategies, many chiral inorganic nanoparticles (NPs) have been prepared and their corresponding optical activity has been explored.[8−10] Generally, chiral inorganic NPs can be obtained by coating chiral organic molecules onto the surface of NPs through either direct use as stabilizers or postsynthetic ligand exchange.[11−16] Among the different types of chiral inorganic NPs, the optical activity of noble metal NPs is most studied. Noble metal NPs with localized surface plasmon resonance (LSPR) can generate strong surface electromagnetic fields, which remarkably influence the optical properties of molecules in proximity to the NPs.[17−22] Reciprocally, the dipole of the chiral molecules near the NP surface can give rise to chiral current inside noble metal NPs, leading to the transportation of chirality from molecules to NPs and the appearance of plasmon-induced circular dichroism (CD) response in the region of visible light.[11,14,15]

Unfortunately, the plasmon-induced CD response of individual noble metal NPs is rather weak; therefore, integration of noble metal NPs is necessary in order to achieve amplified and stronger CD response, which is critical for practical applications of chiral inorganic nanostructures. Especially, one-dimensional (1D) plasmonic assembly, which is able to accommodate the propagation of light arising from near-field coupling between NPs, has the strongest electromagnetic enhancement and is very promising in photonic devices or waveguides.[23−28] Most established strategies rely on the assembly of the noble metal NPs on the 1D template of chiral polymers or biomolecules, in which CD signals of molecules and the LSPR of NPs are both strong.[29−31] However, the utilization of templates has several intrinsic disadvantages with possible sacrifice of physical properties of the materials.[32] In addition, most of current studies of plasmon-induced CD properties are focused on spherical noble metal

* Address correspondence to zytang@nanoctr.cn.

Received for review November 17, 2011 and accepted February 11, 2012.

Published online February 11, 2012
10.1021/nn2044802

NPs with narrow tunable spectral range; therefore, the CD responses are inevitably limited to 400 to 550 nm, and CD signals at longer wavelength were seldom reported. Manipulation of the optical activity across the visible and near-infrared (NIR) light range still remains a great challenge. Herein, we report the optical activity in the templateless 1D assembly of cysteine (CYS) and gold nanorods (GNRs). CD responses can be manipulated on both intensity and wavelength in the range of 500 nm to more than 900 nm by tuning the aspect ratio of the GNRs. Anisotropic enhancement of optical activity is discovered, and the line shape and origin of the CD response are discussed in detail. iIndividual CYS-attached GNRs and CYS-assembled gold nanoparticles (GNPs) substantiate that the form of assembly and the shape of building blocks are significant not only for the intensity but for the line shape of the CD signals.

RESULTS AND DISCUSSION

1D Self-assembly and CD Response of GNRs. Owing to reduced cetyltrimethylammonium bromide (CTAB) stabilizer coverage and high surface energy at the ends of GNRs, addition of CYS molecules into as-prepared GNR solution gives rise to preferential adsorption of CYS onto the ends of GNRs *via* coordination interaction between thiol groups of CYS and the Au surface.[33] Measurement results by high-performance liquid chromatography (HPLC) reveal that there are around 1.33×10^3 CYS molecules on each GNR, suggesting a submonolayer adsorption of CYS at the ends of GNRs (see detailed analysis on p S10, Supporting Information). Subsequently, the two-point electrostatic interaction between amines and carboxylic acids of CYS molecules attached on different GNRs results in 1D assemblies of GNRs at appropriate pH value (Part 1 in the SI and Scheme S1).[34] Experimentally, regardless of addition of L-, D-, or DL-CYS molecules into the GNR solution, the intensity of the longitudinal LSPR absorption band (637 nm) decreases dramatically, and a concomitant formation of a new band at 700 nm shows up; meanwhile, the intensity of the transverse LSPR band is unaffected (Figure 1a). Such characteristic changes in the UV−vis−NIR spectra suggest the formation of 1D self-assembly of GNRs *via* the end-to-end mode.[33,34] The scanning electron microscopy (SEM) image further confirms that most of the GNRs (more than 80%) form 1D assemblies, although random aggregation of GNRs is observed likely due to the evaporation of water (Figure 1b and Figure S2). Meanwhile, such assemblies are always irreversible and resistant to ligand exchange (Figure S3 and the following details).[35]

Interestingly, although three types of 1D assemblies containing L-, D- or DL-CYS, respectively, exhibit identical optical absorption features in the UV−vis−NIR region (Figure 1a), their CD responses in the same region are obviously different (Figure 1c). L- and

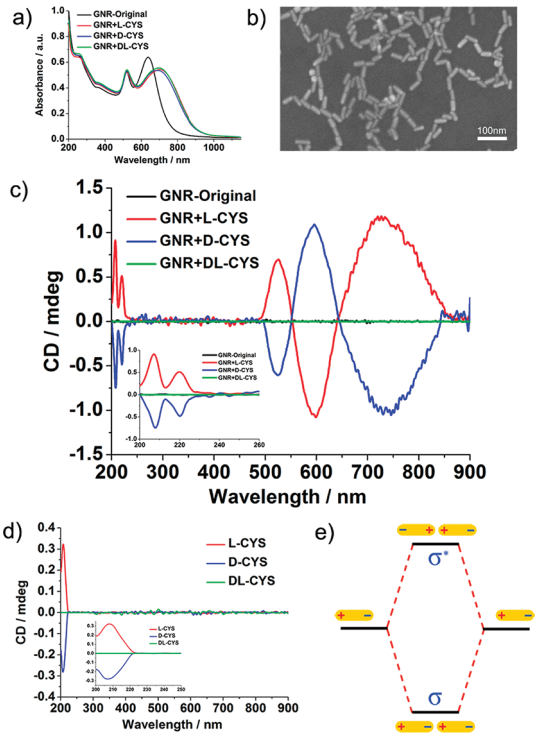

Figure 1. (a) UV−vis−NIR spectra of the original GNRs and 1D self-assembled GNRs formed by three types of CYS; (b) SEM image of the 1D self-assembled GNRs; (c) CD spectra of original GNRs and assembled GNRs by different CYS (inset: CD at 200−260 nm); (d) CD spectra of three types of pure CYS (inset: CD at 200−260 nm); (e) exciton theory scheme of the coupled longitudinal plasmon excitation in the end-to-end assembled GNR dimers.

D-CYS-assembled GNRs present opposite line shape in the CD spectra, whereas DL-CYS assembled GNRs show no chiral effect. In the visible light region, three new peaks at 500−850 nm appear in the CD spectra of CYS and GNR assemblies. The CD peak at around 525 nm can be assigned to the transverse LSPR of the GNRs because of the same position in the UV−vis−NIR spectra (Figure 1a). Another two peaks at 600 and 725 nm exhibit a strong bisignated Cotton effect, which is attributed to the end-to-end arrangement of GNRs in 1D assemblies. The CD response at the plasmon frequency originates from the chiral currents inside the GNRs induced by the dipole of the chiral molecule (CYS) upon the formation of the GNR-CYS complex.[8] Moreover, the bisignated Cotton effect with two peaks at 600 and 725 nm may be explained according to the exciton coupling theory. When the excited-state levels of the GNR split into two levels *via* dimerization, the lower energy level and the higher energy level correspond to two possible arrangements of the transition dipoles formed by the plasmon distribution in the dimer, respectively (Figure 1e).[36,37] As a result, a higher energy antibonding mode at 600 nm (σ^*-peak) and a lower energy peak bonding mode at 725 nm (σ-peak) are formed with a zero crossing point at 640 nm, which is located at a similar position of the

longitudinal LSPR peak of GNRs (637 nm, Figure 1a). It is known that the antibonding plasmon mode generally has no electric field enhancement effect in the gaps of assembled GNRs.[38] However, two assembled GNRs with the connecting angle less than 180° popularly exist in the solution (Figure S2), so there are many CYS molecules attached on the tips of GNRs but not in the gaps of two GNRs. In such regions, the antibonding plasmon mode is explored to determine if it has an electric field enhancement effect, which may cause the plasmon-enhanced CD response.[38] On the other hand, the bonding plasmon mode has an electric field enhancement effect in the gaps of assembled GNRs, so the CYS molecules trapped in the gaps contribute to the CD response of the bonding plasmon mode (σ-peak). As a result, the CD responses induced by both bonding plasmon mode and antibonding plasmon mode are both observed in the visible light region. Meanwhile, the antibonding mode and bonding mode can both have net dipole as long as the connecting angle of the GNR dimers is not 180°. The net dipole may interact with the chiral dipole of the CYS molecule, which results in CD responses in the visible light region.

In the UV region, pure CYS enantiomers have opposite peaks at 200−250 nm in the CD spectra (Figure 1d). As a comparison, L- and D-CYS-assembled GNRs exhibit similar but distinct CD characteristics in the same region.[39,40] First, the spectra generally indicate the same tendency with the corresponding CYS enantiomers (L-CYS is positive and D-CYS is negative). Second, a new CD peak appears at around 220 nm (Figure 1c and inset), which is ascribed to the formation of a Au−S bond.[17] Lastly, the intensity of the CD signal is nearly three times that of the pure CYS in solution at the same concentration. The large electromagnetic field near the CYS molecules generated by GNRs is responsible for the increase of CD intensity of CYS.[41] A recent theoretical study reveals that the plasmon of single noble metal nanomaterials can enhance the molecule's CD signal even if the molecule's UV absorbance is relatively far from the plasmon peak.[8] Furthermore, in our system, the coupling of the plasmon on the tips of GNRs is much stronger than single Au nanocrystals, so it is reasonable that the CD signal of CYS molecules can be enhanced. Accrodingly, as the plasmon intensity increases, the enhancement effect will be more obvious (insets in Figure 2c and d).

Manipulating Intensity and Wavelength of CD Responses. Manipulation of the intensity and wavelength of the plasmon-induced CD response is realized by tuning the aspect ratio of the assembled GNRs (Figure 2). All the experimental parameters including pH,[42] reaction time,[43] temperature, and concentrations of GNRs and CYS[31] are carefully controlled in order to exclude possible side effects. It should be pointed out that for GNRs with the same concentration but with different aspect ratios, the absorbance maxima of the longitudinal LSPR peak present a linear correlation to the

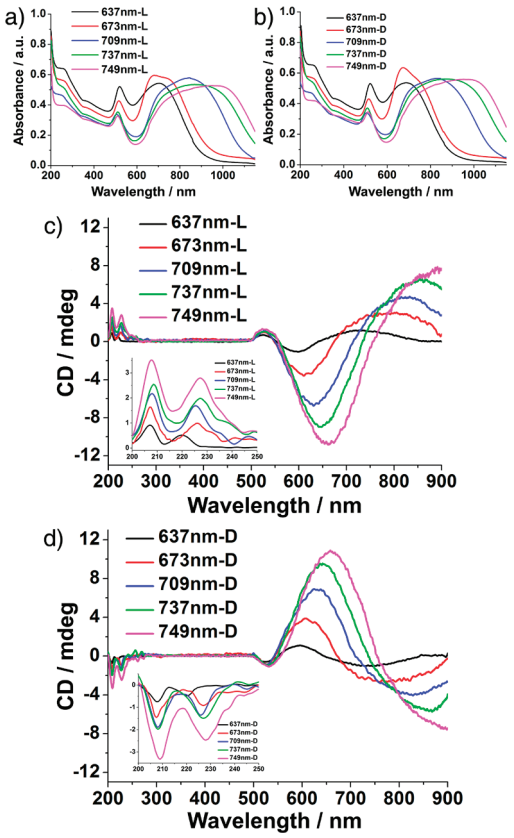

Figure 2. UV−vis−NIR spectra of GNRs with different aspect ratios assembled by L-CYS (a) and D-CYS (b), respectively; (c) and (d) are the corresponding CD response of (a) and (b), respectively (inset: CD spectra at 200−250 nm). Note: The numbers represent the longitudinal LSPR wavelengths of different GNRs; for example, "673 nm-L" stands for the GNRs with the longitudinal LSPR wavelength at 673 nm.

peak wavelength (Figure S5 and Table S1), which is consistent with a previous report.[44] Figure 2c and d indicate the CD responses of the 1D assemblies of CYS and GNRs under the same assembly conditions. Notably, the bisignated CD bands exhibit a gradual bathochromic shift with an increase of the aspect ratios of GNRs in the 1D assembly. The σ^*-peaks and the σ-peaks cover the 550 to 750 nm and 640 nm to NIR wavelength ranges, respectively, fulfilling the manipulation of plasmon-induced CD responses in the visible−NIR light region. We also notice that the σ-peaks at the longer wavelength cannot be fully resolved because of the detection limit of the CD spectrometer (less than 900 nm). So the σ^*-peaks in the visible light region are used for analysis in the below discussion.

Theoretically, the exciton−plasmon coupling between CYS molecules and GNRs is undermined with increasing aspect ratios of GNRs (LSPR peaks of GNRs are bathochromically shifted, gradually away from the absorbance band of CYS molecules located in the UV region), which should result in weaker CD responses. However, Figure 2 and Figures S6 and S7 demonstrate that as the aspect ratios of the GNRs increase, the CD intensities increase in both the UV and visible light

TABLE 1. Anisotropic Factors (AF) of Transverse LSPR and σ^* CD Peaks of L-CYS-Assembled GNRs with Different Aspect Ratios

	TLSPR CD Peak		σ^*-Peak	
	λ/nm	AF/g $\times 10^{-4}$	λ/nm	AF/g $\times 10^{-4}$
GNR-637[a]	526	0.41	598.5	−0.79
GNR-673[a]	525.5	0.73	610.5	−3.07
GNR-709[a]	526	1.13	631	−8.94
GNR-737[a]	525	1.16	647	−10.10
GNR-749[a]	523.5	1.36	661	−11.72

[a] The numbers represent the longitudinal LSPR wavelengths of different GNRs.

region. The opposite tendency in our system reveals that dramatic enhancement of the electromagnetic field in the 1D plasmonic assembly dominates the exciton−plasmon effect. First, as the aspect ratio increases, the LSPR intensity at the end of the GNRs is significantly increased,[45−48] which promotes the chiral currents inside the GNRs induced by the dipole of the CYS. Second, in the 1D assembly, the electromagnetic field is tremendously magnified and "plasmonic nanoantennas" are formed in the gap of adjacent GNRs, which further enhances the CD responses.

Table 1 and Table S2 quantitatively list the anisotropic factors (*g*-factors) of the CD peaks in the 1D assembly. As the aspect ratios of GNRs increase, the increase of the *g*-factors for the σ^* CD peak is much more obvious compared to that of the transverse LSPR CD peak, exhibiting an anisotropic enhancement effect (Table 1). For example, the *g*-factor of the σ^*-peak for GNR-749 is about 15 times as much as that of GNR-637, whereas for the transverse LSPR CD peak, it is only 3 times larger. This result is consistent with the above discussion that in 1D end-to-end assembly the enhancement of electromagnetic fields of GNRs along the longitudinal dimension is more evident than that of the transverse direction. It was suggested that the antisymmetric mode of the two nanowires in the transverse configuration (side by side assembly) can lead to a resonant excitation of the magnetic dipole moment, which is an important mechanism for metamaterials.[49,50] However, in our system, the strong σ^*-peak and obvious anisotropic enhancement were also observed, presenting a promising future for fabricating negative index materials, even if we have not fully discovered the explanation for the phenomenon yet.[13]

CD Responses of CYS-Attached Individual GNRs. The control experiment with the optical activity of individual CYS-attached GNRs confirms that LSPR coupling of the GNRs in a 1D assembly is crucial for generation of intense CD responses (Figure 3). Herein, sodium dodecyl sulfate (SDS) surfactants were introduced to the solution mixture of CYS and GNRs in order to provide enough electrostatic repulsion between CYS-attached GNRs and prevent possible assembly (see experimental details in Part 1 of the SI). Several important features are

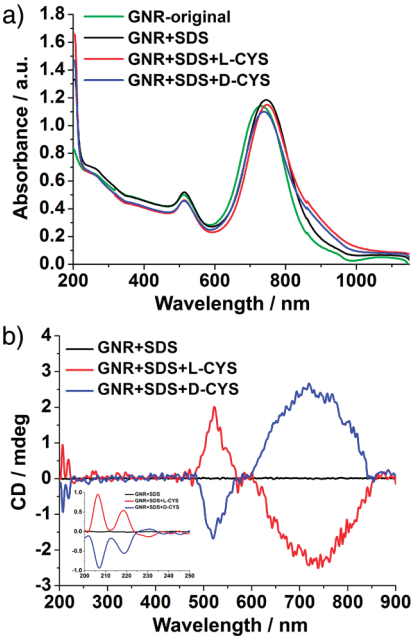

Figure 3. (a) UV−vis−NIR spectra of CYS-attached GNRs in the presence of SDS; (b) corresponding CD spectra of (a) (inset: enlarged CD spectra at 200−250 nm).

discerned: (1) Surface-enhanced Raman scattering (SERS) measurement confirms that CYS molecules are attached on the surface of GNRs (Figure S8); (2) HPLC results show that the adsorption density of CYS molecules is very close to that of the 1D assembly (Figure S9, Table S3); (3) there is no considerable change in UV−vis−NIR spectra, revealing that the CYS-attached GNRs cannot form an assembly in the presence of SDS (Figure 3a); (4) the CD signal in the UV region is identical with that of the 1D assembly (insets in Figure 3b and Figure 1c), which is stronger than that of free CYS molecules in solution (inset in Figure 1c), indicating the enhancement of the electromagnetic field near CYS after attaching to the ends of GNRs; (5) the CD peaks at around 520 and 740 nm are assigned to transverse and longitudinal LSPR, respectively. Evidently, no bisignated CD signals at the longitudinal LSPR are observed, and the corresponding CD response is much weaker comparing to that of the 1D assembled GNRs (−0.67 in Table S4 *vs* −10.10 in Table 1 for *g*-factors of GNRs with similar aspect ratios). The results highlight that the coupling of the LSPR, which enhances the electromagnetic field inside the 1D plasmonic assembly, can not only remarkably influence the intensity of CD response but also change the line shape of the CD signals.

The CD response of individual CYS-attached GNRs indicates that the CD signal originates from plasmon enhancement rather than chiral assembly such as fingers-crossed GNRs.[9] Theoretically, if CYS molecules can induce chiral assembly, individual CYS-attached GNRs rather than 1D assembled GNRs are more likely to form fingers-crossed structures because the motion or spin of individual GNRs is not restricted. In comparison,

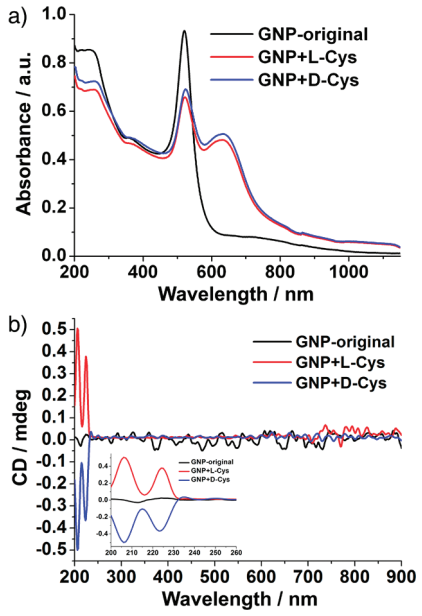

Figure 4. (a) UV–vis–NIR spectra of the GNPs assembled with different CYS; (b) CD spectra of GNPs assembled by L- and D-CYS.

the GNRs in the 1D assembly can be limited by neighboring building blocks so that a strand-like structure instead of a fingers-crossed structure with selective chirality will be formed. However, if a fingers-crossed assembly exists, a bisignate CD response will be observed, which contradicts our results, meaning that individual GNRs cannot realize a chiral assembly let alone the GNRs in a 1D chain. Therefore, the optical activity in our system results from the interaction between chiral dipole and surface plasmon coupling rather than a chiral structure.

CD Responses of CYS-Assembled GNPs. Finally, it is explored that the assembly building blocks and assembly mode are also important factors in generating intense optical activity. In this regard, spherical gold nanoparticles with a LSPR peak at 520 nm are selected (see experimental details in Part 1 of the SI), and the assembly is initiated by addition of CYS molecules with the appearance of a new peak at around 650 nm (Figure 4a). The SEM image demonstrates that such an assembly gives rise to formation of disordered three-dimensional (3D) aggregates (Figure S10). In the CD spectra, the L- and D-CYS-assembled GNPs present mirror-image CD responses in the UV region, but the enhancement effect is obviously weaker than that of GNRs (0.5 mdeg in the inset of Figure 4b *vs* more than 3 mdeg in the insets in Figure 2c and d). In the visible–NIR light region, however, the CD response is nearly absent (Figure 4b). The weak CD responses in the UV and visible light region mainly originate from the relatively weak LSPR intensity of GNPs. Because the SPR region of GNPs (around 520 nm) is relatively far from the CD absorbance of CYS (<220 nm, Figure 1d), the strong SPR intensity of the gold nanocrystals is a prerequisite to the production of CD signals in the visible light region, which is the reason that GNRs can obtain CD response in the visible light region but GNPs cannot. There could be many other factors that possibly influence the CD signals in the visible light region; for example, GNPs with the proper sizes may provide more intense plasmon resonance, the ordered and well-oriented geometry of assembly can contribute to the CD response,[8] while the disordered assembly will counteract the CD signal.[51] Nevertheless, the collective tip-enhanced electromagnetic field in the 1D end-to-end assembly of GNRs, which is absent in the 3D assembly of GNPs, should be the key to produce strong CD responses.

TABLE 2. Volume of Added 10 mM $AgNO_3$ Solution and Corresponding Longitudinal LSPR Wavelengths and Aspect Ratios of the GNRs

	Volume of $AgNO_3$ (μL)				
	240	320	400	480	560
LSPR wavelength (nm)	637	673	709	737	749
aspect ratio	1.72	2.15	2.67	3.30	3.44

CONCLUSION

In conclusion, manipulation of the collective optical activity in the visible–NIR region is realized by taking advantage of the 1D assembly of CYS and GNRs. The anisotropic enhancement of the CD responses is explored and studied in detail. These results give new insight into chiral photonics and provide a possible route for the applications of chiral materials and devices.

METHODS

Synthesis of GNRs. The GNRs were prepared by the "seed-mediated growth method" according to the report with slight modification.[52,53] Briefly, 250 μL of 10 mM $HAuCl_4$ solution was added to 7.5 mL of a 100 mM CTAB solution at 30 °C. After gentle mixing, 0.6 mL of a 10 mM ice-cold $NaBH_4$ solution and 1.65 mL of water were added, followed by rapid stirring for 2 min. The CTAB-capped gold seed solution was stored at 30 °C for 2 h. In sequence, 4 mL of 10 mM $HAuCl_4$ solution, 480 μL of 10 mM $AgNO_3$ solution, 480 μL of a freshly prepared 100 mM ascorbic acid solution, and 96 μL of CTAB-capped gold seed solution were added to 80 mL of 100 mM CTAB solution at 30 °C. The solution was thoroughly mixed after each addition. Finally, the gold nanorod solution was left undisturbed and aged for 12 h. The samples were purified by centrifugation (12 000 rpm, 10 min) three times and redispersed in water. The aspect ratios of the GNRs could be tuned by changing the content of $AgNO_3$ (Table 2).

Synthesis of GNPs. The GNPs were synthesized by converting the overgrown GNRs to GNPs as we reported previously.[54] An 80 mL portion of the as-synthesized gold nanorod solution was centrifuged (12 000 rpm, 10 min) and redispersed in water. Subsequently, the solution was centrifuged (12 000 rpm,

10 min) again and redispersed in 80 mL of 10 mM CTAB solution at 40 °C. Then, 4 mL of 10 mM $HAuCl_4$ solution and 0.8 mL of 100 mM ascorbic acid solution were added in sequence and mixed thoroughly. The mixture was allowed to react at 40 °C for 1 h. The overgrown gold nanorod solution was centrifuged (12 000 rpm, 10 min) and redispersed in 80 mL of 10 mM CTAB solution. Next, at 40 °C, 1.6 mL of 10 mM $HAuCl_4$ solution was added. After the solution was gently mixed, it was left undisturbed and aged for 12 h. The solution was then washed three times by centrifugation (12 000 rpm, 10 min) and finally dispersed in water.

1D Self-Assembly of GNRs. 1D self-assembly of GNRs was initiated by the ligand exchange reaction between CYS and CTAB on the ends of GNRs. Briefly, 0.7 mL of a 50 μM CYS solution was added into 6.3 mL of GNR solution at 25 °C, and the pH value was adjusted to 6.0. The solution was subjected to CD or UV−vis−NIR measurement immediately after stirring for 30 s. Self-assembly of GNPs was initiated by the ligand exchange reaction between CYS and CTAB on the surface of GNPs. The sample preparation was the same as the self-assembly of GNRs.

Preparation of Individual CYS-Attached GNRs. Individual CYS-attached GNRs were prepared by simultaneously coating SDS on GNRs. A 70 μL amount of 0.1% SDS (mass fraction) was added to 6.3 mL of GNR solution at 25 °C. To attach CYS onto the surface of GNRs, 0.7 mL of 50 μM CYS was added into the mixture solution in sequence. The pH value of the final solution was adjusted to 11.5 by NaOH so that CYS could not assemble GNRs with a two-point electrostatic interaction between amines and carboxylic acids, because this pH value was beyond the pK_3 of CYS, which was high enough to ensure the attachment of thiols to the GNRs. The samples were subject to characterization after leaving undisturbed for 12 h.

Instrumentation. CD spectra were recorded by a Jasco J-810 spectropolarimeter in aqueous solution. A 3 mL portion of each sample was infused into a 1 cm quartz cell and measured at the scan speed of 500 nm/min with a bandwidth of 10 nm. Accumulation was conducted three times continuously for each sample. UV−vis−NIR absorption measurements were carried out using a Lambda 950 UV−vis−NIR spectrometer, and the method for preparing the each sample was the same as the CD measurements.

In surface-enhanced Raman spectroscopy measurements, 0.5 mL of the solution of single GNRs was dropped onto a 0.5 cm × 1 cm silicon wafer for full drying. Raman spectra excited with a 633 nm laser line were acquired with a Renishaw InVia System spectrometer coupled to a Leica microscope. The laser power was set to 1% of the full power. The laser beam was focused on the sample by a 50× objective lens (NA = 0.75). The spectra were measured at 1 cm^{-1} resolution with an exposure time of 4 s.

Scanning electron microscopy images of single GNRs, self-assembled GNRs, and GNPs were obtained using a Hitachi S-4800 SEM operating at 30 kV. The prepared samples were dropped onto silicon wafers and observed after complete drying.

Conflict of Interest: The authors declare no competing financial interest.

Acknowledgment. This work was partially supported by the National Natural Science Foundation for Distinguished Youth Scholars of China (21025310, Z.Y.T.), National Natural Science Foundation of China (21003026, Y.G.; 20973047 and 91027011, Z.Y.T.), National Research Fund for Fundamental Key Project (2009CB930401, Z.Y.T.), and 100 Talent Program of Chinese Academy of Sciences (Z.Y.T.).

Supporting Information Available: TEM images and aspect ratio distribution of different GNRs (Figure S1); scheme and SEM image of end-to-end assembly of GNRs (Scheme S1 and Figure S2); UV and CD spectra to prove the irreversibility of the assembly (Figure S3); UV spectra of pure CYS (Figure S4); determination of the concentration of GNRs with different aspect ratios (Figure S5 and Table S1); comprehensive UV−vis−NIR and CD spectra of original GNRs and assembled GNRs with different aspect ratios (Figures S6 and S7); calculation of *g*-factors of D-CYS-assembled GNRs with different aspect ratios (Table S2); SERS spectra to comfirm Au−S bond in individual CYS-attached GNRs (Figure S8); calculation comfirming the submonolayer of CYS molecules on the surface of GNRs (Figure S9, Table S3, pp S10 to S11); *g*-factors of individual CYS-attached GNRs (Table S4); SEM images of CYS-assembled GNPs (Figure S10). This material is available free of charge *via* the Internet at http://pubs.acs.org.

REFERENCES AND NOTES

1. Nan, J.; Yan, X. P. A Circular Dichroism Probe for L-Cysteine Based on the Self-Assembly of Chiral Complex Nanoparticles. *Chem.—Eur. J.* **2010**, *16*, 423–427.
2. Shukla, N.; Bartel, M. A.; Gellman, A. J. Enantioselective Separation on Chiral Au Nanoparticles. *J. Am. Chem. Soc.* **2010**, *132*, 8575–8580.
3. Sivaguru, J.; Poon, T.; Franz, R.; Jockusch, S.; Adam, W.; Turro, N. J. Stereocontrol within Confined Spaces: Enantioselective Photooxidation of Enecarbamates inside Zeolite Supercages. *J. Am. Chem. Soc.* **2004**, *126*, 10816–10817.
4. Pendry, J. B. A Chiral Route to Negative Refraction. *Science* **2004**, *306*, 1353–1355.
5. Zhang, J.; Albelda, M. T.; Liu, Y.; Canary, J. W. Chiral Nanotechnology. *Chirality* **2005**, *17*, 404–418.
6. Li, Y.; Zhou, Y.; Wang, H.-Y.; Perrett, S.; Zhao, Y.; Tang, Z.; Nie, G. Chirality of Glutathione Surface Coating Affects the Cytotoxicity of Quantum Dots. *Angew. Chem., Int. Ed.* **2011**, *50*, 5860–5864.
7. Xia, Y.; Zhou, Y.; Tang, Z. Chiral Inorganic Nanoparticles: Origin, Optical Properties and Bioapplications. *Nanoscale* **2011**, *3*, 1374–1382.
8. Govorov, A. O.; Fan, Z. Y.; Hernandez, P.; Slocik, J. M.; Naik, R. R. Theory of Circular Dichroism of Nanomaterials Comprising Chiral Molecules and Nanocrystals: Plasmon Enhancement, Dipole Interactions, and Dielectric Effects. *Nano Lett.* **2010**, *10*, 1374–1382.
9. Auguie, B.; Alonso-Gomez, J. L.; Guerrero-Martinez, A.; Liz-Marzan, L. M. Fingers Crossed: Optical Activity of a Chiral Dimer of Plasmonic Nanorods. *J. Phys. Chem. Lett.* **2011**, *2*, 846–851.
10. Govorov, A. O. Plasmon-Induced Circular Dichroism of a Chiral Molecule in the Vicinity of Metal Nanocrystals. Application to Various Geometries. *J. Phys. Chem. C* **2011**, *115*, 7914–7923.
11. Gautier, C.; Burgi, T. Chiral Gold Nanoparticles. *ChemPhysChem* **2009**, *10*, 483–492.
12. Gautier, C.; Burgi, T. Chiral Inversion of Gold Nanoparticles. *J. Am. Chem. Soc.* **2008**, *130*, 7077–7084.
13. Gansel, J. K.; Thiel, M.; Rill, M. S.; Decker, M.; Bade, K.; Saile, V.; von Freymann, G.; Linden, S.; Wegener, M. Gold Helix Photonic Metamaterial as Broadband Circular Polarizer. *Science* **2009**, *325*, 1513–1515.
14. Lieberman, I.; Shemer, G.; Fried, T.; Kosower, E. M.; Markovich, G. Plasmon-Resonance-Enhanced Absorption and Circular Dichroism. *Angew. Chem. Int. Ed.* **2008**, *47*, 4855–4857.
15. Rezanka, P.; Zaruba, K.; Kral, V. Supramolecular Chirality of Cysteine Modified Silver Nanoparticles. *Colloid Surf. A* **2011**, *374*, 77–83.
16. Slocik, J. M.; Govorov, A. O.; Naik, R. R. Plasmonic Circular Dichroism of Peptide-Functionalized Gold Nanoparticles. *Nano Lett.* **2011**, *11*, 701–705.
17. Huang, X. H.; Neretina, S.; El-Sayed, M. A. Gold Nanorods: From Synthesis and Properties to Biological and Biomedical Applications. *Adv. Mater.* **2009**, *21*, 4880–4910.
18. Zhu, Z.; Meng, H.; Liu, W.; Liu, X.; Gong, J.; Qiu, X.; Jiang, L.; Wang, D.; Tang, Z. Superstructures and SERS Properties of Gold Nanocrystals with Different Shapes. *Angew. Chem., Int. Ed.* **2011**, *50*, 1593–1596.
19. Mirkin, C. A. Programming the Assembly of Two- and Three-Dimensional Architectures with DNA and Nanoscale Inorganic Building Blocks. *Inorg. Chem.* **2000**, *39*, 2258–2272.
20. Feng, M.; Zhang, M.; Song, J. M.; Li, X. G.; Yu, S. H. Ultralong Silver Trimolybdate Nanowires: Synthesis, Phase Transformation, Stability, and Their Photocatalytic,

Optical, and Electrical Properties. *ACS Nano* **2011**, *5*, 6726–6735.
21. Sun, Y. G.; Wang, Y. X. Monitoring of Galvanic Replacement Reaction between Silver Nanowires and HAuCl(4) by *in Situ* Transmission X-ray Microscopy. *Nano Lett.* **2011**, *11*, 4386–4392.
22. Wang, D. Y. Supraparticle Physical Chemistry. *Phys. Chem. Chem. Phys.* **2010**, *12*, 11819–11820.
23. Barnes, W. L.; Dereux, A.; Ebbesen, T. W. Surface Plasmon Subwavelength Optics. *Nature* **2003**, *424*, 824–830.
24. Maier, S. A.; Kik, P. G.; Atwater, H. A.; Meltzer, S.; Harel, E.; Koel, B. E.; Requicha, A. A. G. Local Detection of Electromagnetic Energy Transport below the Diffraction Limit in Metal Nanoparticle Plasmon Waveguides. *Nat. Mater.* **2003**, *2*, 229–232.
25. Halas, N. J. Plasmonics: An Emerging Field Fostered by Nano Letters. *Nano Lett.* **2010**, *10*, 3816–3822.
26. Nie, Z. H.; Petukhova, A.; Kumacheva, E. Properties and Emerging Applications of Self-Assembled Structures Made from Inorganic Nanoparticles. *Nat. Nanotechnol.* **2010**, *5*, 15–25.
27. Antonietti, M.; Niederberger, M.; Smarsly, B. Self-Assembly in Inorganic and Hybrid Systems: Beyond the Molecular Scale. *Dalton Trans.* **2008**, 18–24.
28. Yang, M.; Chen, G.; Zhao, Y.; Silber, G.; Wang, Y.; Xing, S.; Han, Y.; Chen, H. Mechanistic Investigation into the Spontaneous Linear Assembly of Gold Nanospheres. *Phys. Chem. Chem. Phys.* **2010**, *12*, 11850–11860.
29. Guerrero-Martinez, A.; Auguie, B.; Alonso-Gomez, J. L.; Dzolic, Z.; Gomez-Grana, S.; Zinic, M.; Cid, M. M.; Liz-Marzan, L. M. Intense Optical Activity from Three-Dimensional Chiral Ordering of Plasmonic Nanoantennas. *Angew. Chem., Int. Ed.* **2011**, *50*, 5499–5503.
30. Qi, H. Q.; Shopsowitz, H.; Hamad, K. E.; MacLachlan, W. Y.; Chiral, M. J. Nematic Assemblies of Silver Nanoparticles in Mesoporous Silica Thin Films. *J. Am. Chem. Soc.* **2011**, *133*, 3728–3731.
31. Oh, H. S.; Liu, S.; Jee, H.; Baev, A.; Swihart, M. T.; Prasad, P. N. Chiral Poly(fluorene-alt-benzothiadiazole) (PFBT) and Nanocomposites with Gold Nanoparticles: Plasmonically and Structurally Enhanced Chirality. *J. Am. Chem. Soc.* **2010**, *132*, 17346–17348.
32. Tang, Z. Y.; Kotov, N. A. One-Dimensional Assemblies of Nanoparticles: Preparation, Properties, and Promise. *Adv. Mater.* **2005**, *17*, 951–962.
33. Wang, Y.; DePrince, A. E.; Gray, S. K.; Lin, X. M.; Pelton, M. Solvent-Mediated End-to-End Assembly of Gold Nanorods. *J. Phys. Chem. Lett.* **2010**, *1*, 2692–2698.
34. Sudeep, P. K.; Joseph, S. T. S.; Thomas, K. G. Selective Detection of Cysteine and Glutathione Using Gold Nanorods. *J. Am. Chem. Soc.* **2005**, *127*, 6516–6517.
35. Chen, T.; Wang, H.; Chen, G.; Wang, Y.; Feng, Y. H.; Teo, W. S.; Wu, T.; Chen, H. Y. Hotspot-Induced Transformation of Surface-Enhanced Raman Scattering Fingerprints. *ACS Nano* **2010**, *4*, 3087–3094.
36. Jain, P. K.; Eustis, S.; El-Sayed, M. A. Plasmon Coupling in Nanorod Assemblies Optical Absorption, Discrete Dipole Approximation Simulation, and Exciton-Coupling Model. *J. Phys. Chem. B* **2006**, *110*, 18243–18253.
37. Slaughter, L. S.; Wu, Y.; Willingham, B. A.; Nordlander, P.; Link, S. Effects of Symmetry Breaking and Conductive Contact on the Plasmon Coupling in Gold Nanorod Dimers. *ACS Nano* **2010**, *4*, 4657–4666.
38. Shao, L.; Woo, K. C.; Chen, H. J.; Jin, Z.; Wang, J. F.; Lin, H. Q. Angle- and Energy-Resolved Plasmon Coupling in Gold Nanorod Dimers. *ACS Nano* **2010**, *4*, 3053–3062.
39. Zhou, Y. L.; Yang, M.; Sun, K.; Tang, Z. Y.; Kotov, N. A. Similar Topological Origin of Chiral Centers in Organic and Nanoscale Inorganic Structures: Effect of Stabilizer Chirality on Optical Isomerism and Growth of CdTe Nanocrystals. *J. Am. Chem. Soc.* **2010**, *132*, 6006–6013.
40. Li, T.; Park, H. G.; Lee, H.-S.; Choi, S.-H. Circular Dichroism Study of Chiral Biomolecules Conjugated with Silver Nanoparticles. *Nanotechnology* **2004**, *15*, S660–S663.
41. Lee, A.; Andrade, G. F. S.; Ahmed, A.; Souza, M. L.; Coombs, N.; Tumarkin, E.; Liu, K.; Gordon, R.; Brolo, A. G.; Kumacheva, E. Probing Dynamic Generation of Hot-Spots in Self-Assembled Chains of Gold Nanorods by Surface-Enhanced Raman Scattering. *J. Am. Chem. Soc.* **2011**, *133*, 7563–7570.
42. Sun, Z. H.; Ni, W. H.; Yang, Z.; Kou, X. S.; Li, L.; Wang, J. F. pH-Controlled Reversible Assembly and Disassembly of Gold Nanorods. *Small* **2008**, *4*, 1287–1292.
43. Thomas, K. G.; Barazzouk, S.; Ipe, B. I.; Joseph, S. T. S.; Kamat, P. V. Uniaxial Plasmon Coupling through Longitudinal Self-Assembly of Gold Nanorods. *J. Phys. Chem. B* **2004**, *108*, 13066–13068.
44. Orendorff, C. J.; Murphy, C. J. Quantitation of Metal Content in the Silver-Assisted Growth of Gold Nanorods. *J. Phys. Chem. B* **2006**, *110*, 3990–3994.
45. Hooshmand, N.; Jain, P. K.; El-Sayed, M. A. Plasmonic Spheroidal Metal Nanoshells Showing Larger Tunability and Stronger Near Fields Than Their Spherical Counterparts: An Effect of Enhanced Plasmon Coupling. *J. Phys. Chem. Lett.* **2011**, *2*, 374–378.
46. Myroshnychenko, V.; Rodriguez-Fernandez, J.; Pastoriza-Santos, I.; Funston, A. M.; Novo, C.; Mulvaney, P.; Liz-Marzan, L. M.; de Abajo, F. J. G. Modelling the Optical Response of Gold Nanoparticles. *Chem. Soc. Rev.* **2008**, *37*, 1792–1805.
47. Zuloaga, J.; Prodan, E.; Nordlander, P. Quantum Plasmonics: Optical Properties and Tunability of Metallic Nanorods. *ACS Nano* **2010**, *4*, 5269–5276.
48. Bryant, G. W.; De Abajo, F. J. G.; Aizpurua, J. Mapping the Plasmon Resonances of Metallic Nanoantennas. *Nano Lett.* **2008**, *8*, 631–636.
49. Halas, N. J.; Lal, S.; Chang, W. S.; Link, S.; Nordlander, P. Plasmons in Strongly Coupled Metallic Nanostructures. *Chem. Rev.* **2011**, *111*, 3913–3961.
50. Liu, N.; Giessen, H. Coupling Effects in Optical Metamaterials. *Angew. Chem., Int. Ed.* **2010**, *49*, 9838–9852.
51. Fan, Z. Y.; Govorov, A. O. Plasmonic Circular Dichroism of Chiral Metal Nanoparticle Assemblies. *Nano Lett.* **2010**, *10*, 2580–2587.
52. Nikoobakht, B.; El-Sayed, M. A. Preparation and Growth Mechanism of Gold Nanorods (NRs) Using Seed-Mediated Growth Method. *Chem. Mater.* **2003**, *15*, 1957–1962.
53. Sau, T. K.; Murphy, C. J. Seeded High Yield Synthesis of Short Au Nanorods in Aqueous Solution. *Langmuir* **2004**, *20*, 6414–6420.
54. Niu, W. X.; Zheng, S. L.; Wang, D. W.; Liu, X. Q.; Li, H. J.; Han, S. A.; Chen, J.; Tang, Z. Y.; Xu, G. B. Selective Synthesis of Single-Crystalline Rhombic Dodecahedral, Octahedral, and Cubic Gold Nanocrystals. *J. Am. Chem. Soc.* **2009**, *131*, 697–703.